

RESEARCH ARTICLE | MAY 28 2025

Development of millimeter-thick hexagonal boron nitride wafers and fast neutron detectors

G. Somasundaram ; N. K. Hossain ; Z. Alemoush ; A. Tingsuwatit ; J. Li ; J. Y. Lin ; H. X. Jiang 

 Check for updates

Appl. Phys. Lett. 126, 212104 (2025)

<https://doi.org/10.1063/5.0274262>



View Online



Export Citation

Articles You May Be Interested In

Annealing effects on crystalline quality and device performance of ultrawide bandgap h-BN quasi-bulk crystals

Appl. Phys. Lett. (May 2025)

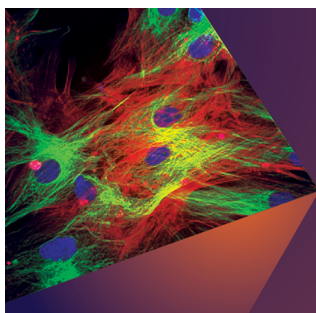
Transport properties of h-BN lateral devices

Appl. Phys. Lett. (January 2025)

Toward achieving cost-effective hexagonal BN semi-bulk crystals and BN neutron detectors via halide vapor phase epitaxy

Appl. Phys. Lett. (January 2023)

28 May 2025 16:00:43



Applied Physics Letters

Special Topics Open for Submissions

[Learn More](#)

Development of millimeter-thick hexagonal boron nitride wafers and fast neutron detectors

Cite as: Appl. Phys. Lett. **126**, 212104 (2025); doi: [10.1063/5.0274262](https://doi.org/10.1063/5.0274262)

Submitted: 4 April 2025 · Accepted: 14 May 2025 ·

Published Online: 28 May 2025



View Online



Export Citation



CrossMark

G. Somasundaram,^{a)} N. K. Hossain, Z. Alemoush, A. Tingsuwatit, J. Li, J. Y. Lin, and H. X. Jiang

AFFILIATIONS

Department of Electrical and Computer Engineering, Texas Tech University, Lubbock, Texas 79409, USA

^{a)} Author to whom correspondence should be addressed: gsomasun@ttu.edu

ABSTRACT

We report the attainment of millimeter-thick neutron detectors fabricated from quasi-bulk hexagonal boron nitride (*h*-BN) produced by halide vapor phase epitaxy (HVPE). Detection efficiencies of 0.7% and 0.5% in response to neutrons emitted from bare AmBe and Cf-252 sources, respectively, have been achieved, corresponding to a charge collection efficiency of about 38%. These results mark a significant improvement over our previous single-stack *h*-BN detectors, which were 90 μm thick and exhibited a detection efficiency of 0.1%. This enhancement is primarily attributed to the increased thickness of the *h*-BN layer, leading to a higher intrinsic detection efficiency. We also observed that the carrier mobility-lifetime ($\mu\tau$) product increases as layers of *h*-BN are successively removed from the top by polishing, indicating that a degradation in *h*-BN's electronic properties with thickness is now a major limiting factor for achieving high charge collection efficiency. This finding highlights the need for further refinement in HVPE growth processes to produce *h*-BN wafers with both larger thicknesses and improved electronic properties. Nevertheless, the fabrication of millimeter-thick single-stack *h*-BN neutron detectors represents a major milestone in the application of *h*-BN for fast neutron detection.

Published under an exclusive license by AIP Publishing. <https://doi.org/10.1063/5.0274262>

Hexagonal boron nitride (*h*-BN) has garnered significant research interest due to its exceptional properties. Monolayers and few layers are extensively explored as templates, barriers, passivation layers, gate materials for two-dimensional (2D) structures,¹ and a host for optically stable single-photon emitters.² In its 3D form, *h*-BN exhibits extraordinary physical properties, including an ultrawide bandgap (UWBG) of ~6 eV,^{3–7} a high breakdown field of ~12 MV/cm,^{8,9} and high in-plane thermal conductivity of ~550 W/m·K.¹⁰ These combined attributes make bulk *h*-BN a compelling UWBG material for a wide range of applications. Substantial progress has been achieved in synthesizing large-area *h*-BN thin epitaxial films via techniques such as metal-organic chemical vapor deposition (MOCVD),^{11,12} molecular beam epitaxy (MBE),^{13–15} and chemical vapor deposition.¹⁶ Nevertheless, current bulk crystal growth methods, including high-pressure and high-temperature (HPHT)^{4–9} and metal flux solution approaches,^{6,10} are limited to producing millimeter-sized crystals with inherent limitations in scaling to larger wafer dimensions. Therefore, a critical gap persists in the development of *h*-BN materials that simultaneously exhibit large-scale dimensions, significant thickness, and high crystalline quality and purity, which are essential for realizing more complex and advanced device functionalities.

Moreover, *h*-BN containing the isotope B-10 is highly effective for thermal neutron detection due to B-10's unusually large

thermal neutron absorption cross section, approximately 3840 barns ($=3.84 \times 10^{-21} \text{ cm}^2$).^{17,18} This property enables the creation of direct-conversion solid-state thermal neutron detectors. Achieving high efficiency *h*-BN thermal neutron detector requires a substantial layer thickness (d) due to the characteristics of thermal neutron absorption in *h*-BN,¹¹

$$\eta_i = 1 - e^{-\frac{d}{\lambda}}, \quad (1)$$

where η_i denotes the intrinsic detection efficiency, d is the detector's thickness, and λ is the neutron absorption length with $\lambda = 47.3 \mu\text{m}$ for B-10 enrich *h*-BN (*h*-¹⁰BN).^{11,19–22} We have realized *h*-BN direct conversion thermal neutron detectors with a detection area of 1 cm² and a record detection efficiency of 60% using 100 μm thick *h*-¹⁰BN wafers.^{21,22} Conversely, the use of natural boron sources that contain 20% of B-10 and 80% of B-11 for fabricating high efficiency *h*-BN thermal neutron detectors is economically preferred but necessitates the development of *h*-BN with significantly increased thickness, as the thermal neutron absorption length in natural *h*-BN ($\lambda = 237 \mu\text{m}$) is five times larger than that in *h*-¹⁰BN.

Developing a single material sensitive to both thermal and fast neutrons is valuable for advancing neutron detection technologies. However, directly detecting fast neutrons (energies above 1 MeV)

remains a significant challenge due to their extremely low interaction cross section with matter. This low probability of interaction makes it difficult to achieve sufficient detection efficiency without using hydrogen-rich moderating materials, like high-density polyethylene (HDPE), to first thermalize the neutrons. Currently, no effective method exists for the direct detection of fast neutrons with adequate efficiency.

Unlike thermal neutron detection, which relies on the nuclear reaction between thermal neutrons and B-10, the direct detection of fast neutrons using *h*-BN primarily involves elastic scattering of fast neutrons with atomic constituents (B-10, B-11, and N-14). The recoiling ions produced by this scattering process then generate free charge carriers within *h*-BN. The intrinsic detection efficiency (η_i) of a fast neutron detector as a function of *h*-BN thickness also follows Eq. (1), with λ denoting the neutron mean free path of the elastic scattering process. The interaction probabilities of fast neutrons with B-10, B-11, and N are all similar and decrease with an increase in neutron energy (E_N) and have a typical cross section of about ~ 1.3 barn at $E_N > 1$ MeV.^{18,23,24} The atomic densities of B and N in *h*-BN are 5.5×10^{22} cm⁻³. These data together provide a mean free path (λ) of fast neutrons in *h*-BN of a few centimeters. The experimentally measured λ in *h*-BN is 5.2 and 7.6 cm for fast neutrons from AmBe source and Cf-252 source, respectively.²⁵

Based on Eq. (1), the primary challenge for achieving high-efficiency *h*-BN fast neutron detectors is to produce wafers that are sufficiently thick (at least a fraction of λ) while maintaining high crystalline quality for effective charge collection. Meeting both requirements simultaneously is highly challenging. Previously, we demonstrated 0.1% detection efficiency for fast neutrons emitted from a bare Cf-252 neutron source using a single-stack 90 μ m thick *h*-BN detector.²⁶ More recently, stacking multiple 350 μ m-thick detectors improved efficiencies to 2.2% and 0.5% for bare AmBe and Cf-252 sources, respectively.²⁵ Here, we report significant progress with the attainment of a single-stack 1 mm thick *h*-BN fast neutron detector. Via a layer-by-layer polishing approach, we also showed that charge collection efficiency is affected by a decline in the carrier mobility-lifetime ($\mu\tau$) product as material thickness increases.

The 1 mm thick quasi-bulk *h*-BN wafer was grown on 4"-diameter *c*-plane sapphire by HVPE at a growth temperature of 1500 °C using natural boron trichloride (BCl₃) and ammonia (NH₃) as precursors for B and N, respectively. A low-temperature *h*-BN buffer layer is initially grown to mitigate mismatches between lattice constant and thermal expansion coefficient (TEC) differences between *h*-BN and sapphire. At a growth temperature of 1500 °C, the growth rate was about 20 μ m/h. Due to its layered crystalline structure, *h*-BN self-separates from sapphire to form a freestanding wafer during the cooling process after growth.^{21,22,25–27}

Figure 1 shows x-ray diffraction (XRD) pattern in $2\theta - \theta$ scan of a 1 mm thick freestanding *h*-BN quasi-bulk wafer synthesized by HVPE, revealing the *h*-BN (002) peak position (diffraction from stacked planes in the *c*-direction) centered at $2\theta = 26.56^\circ$, corresponding to a *c*-lattice constant of approximately 6.70 Å. Phase pure *h*-BN has a *c*-lattice constant of 6.66 Å, corresponding to the (002) peak in the $2\theta - \theta$ spectrum of 26.75°. The observed $2\theta - \theta$ position at 26.56° in the 1 mm thick *h*-BN wafer deviates more from the ideal position in comparison with those observed in bulk crystals produced by HTHP and metal flux solution methods as well as in our 100 μ m

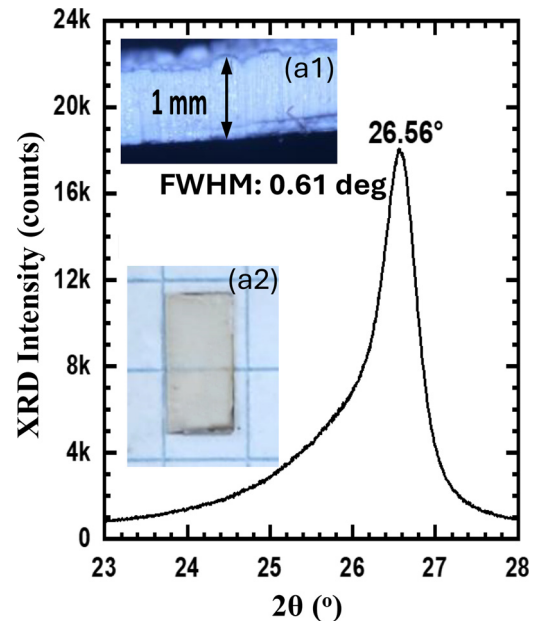


FIG. 1. X-ray diffraction (XRD) pattern in a $2\theta - \theta$ scan of a 1 mm thick freestanding *h*-BN wafer synthesized by HVPE. Insets (a1) and (a2) show the cross-sectional image and the top view of a sample diced from the as-grown 1 mm thick *h*-BN wafer, respectively.

thick *h*-BN HVPE grown wafers.²² Moreover, the full width at half-maximum (FWHM) of the (002) peak (FWHM = 0.61°) is substantially broader than that observed in 100 μ m thick *h*-BN HVPE grown wafers (FWHM = 0.29°).²² The comparison XRD result indicates a reduced structural order of the 1 mm thick *h*-BN wafer here. The inset (a1) is an optical image of the cross-sectional view of the as-grown 1 mm thick freestanding *h*-BN. This wafer exhibits a reasonable transparency as seen in the inset (a2), attributing to the use of carbon-free precursors in HVPE growth.

Due to its layered crystalline structure, most physical properties of *h*-BN are anisotropic. The measured carrier mobility-lifetime ($\mu\tau$) products in the lateral direction (*c*-plane) are two orders of magnitude larger than those in the vertical direction (*c*-axis) for both electrons and holes.^{11,20} Therefore, photoconductive-type detectors were fabricated in a lateral geometry to leverage the superior lateral transport properties of *h*-BN. The optical image in Fig. 2(a) displays a lateral detector fabricated from the 1 mm thick *h*-BN wafer before packaging. The fabrication process involves the following steps: (1) *h*-BN strips with dimensions of 1.3×5 mm were diced from the wafer and mounted on sapphire using polyamide adhesive (as marked in red color); (2) shadow masks with respective dimensions were fabricated and used to deposit metal contacts of bilayers Ni (100 nm)/Au (40 nm) at the two edges of the *h*-BN strips using e-beam evaporation; and (3) metal contacts were deposited along both edges of the *h*-BN strip with a width of 0.15 mm, leaving a 1 mm spacing between the two electrodes. Figure 2(b) shows an image of a fabricated 1 mm-thick *h*-BN lateral detector mounted in a dual-in-line package (DIP) for electrical properties and neutron detection efficiency characterization.

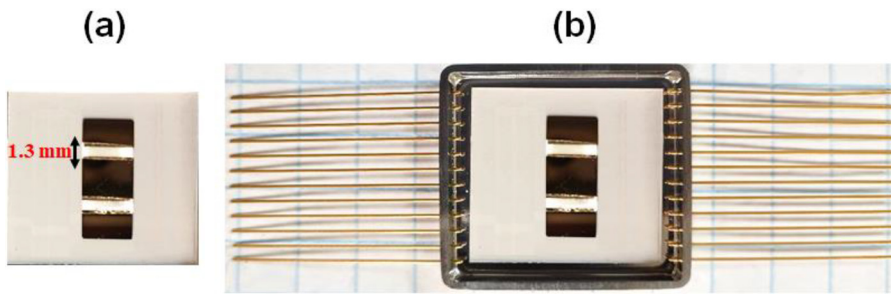


FIG. 2. (a) Optical image of the 1 mm-thick *h*-BN device ($1.3 \times 5 \text{ mm}^2$), mounted on a polyamide adhesive following metal deposition. (b) Micrograph of the *h*-BN neutron detector in a package.

Figure 3(a) plots the current–voltage (*I*–*V*) characteristics of the 1 mm thick *h*-BN device measured in the dark. A linear fit provides a dark electric resistivity of $2.4 \times 10^{14} \Omega \text{ cm}$, which is comparable to the values of *h*-BN materials produced previously by HVPE and MOCVD.^{11,20–22,25–27} The carrier mobility–lifetime product ($\mu\tau$) plays a pivotal role in determining the transport properties and hence the charge collection efficiency of *h*-BN devices. To ensure that most of the charge carriers generated are collected by the electrodes, the recombination lifetime (τ) must be longer than the transit time (τ_t), expressed as $\tau \gg \tau_t$. This charge collection condition also implies that charge carrier drift length ($\mu\tau E$) must be greater than the carrier transit distance (width of detector strip *W*), expressed as $\mu\tau E \gg W$, or

$$V \gg \frac{W^2}{\mu\tau}. \quad (2)$$

For a given *W*, higher $\mu\tau$ values allow for lower applied fields (*E*) or voltages (*V*) to ensure a high charge collection efficiency. Since $\mu\tau$ is determined by material quality and purity, tracking its progress is an effective approach in guiding the development of *h*-BN materials and improving the performance of high-efficiency neutron detectors.

The bias voltage dependence of the photocurrent was measured under uniform illumination, using a broad light source with wavelengths ranging from 185 to 400 nm. This wavelength range encompasses both band-to-band and impurity-to-band charge carrier excitation in *h*-BN. Figure 3(b) shows the measured photocurrent

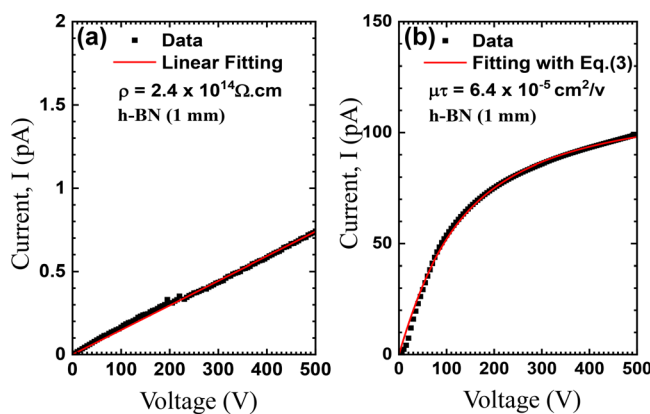


FIG. 3. (a) *I*–*V* characteristics (solid squares) of the 1 mm thick *h*-BN detector measured in the dark, with a linear fit (red curves); (b) measured applied voltage dependence of photocurrent (solid squares) and least squares fitting (red curves) using Eq. (3) for the 1 mm thick *h*-BN detectors.

(solid squares) as a function of applied bias voltage for the device. Based on the classical Many’s equation, we have provided a modified description for the bias voltage dependence of the photocurrent in UWBG materials,²⁷

$$I(V) = (I_0 \mu\tau V / W^2) [1 - (1 - a)(\mu\tau V / W^2)(1 - \exp(-W^2 / \mu\tau V))]. \quad (3)$$

Here, I_0 is the scaling factor that represents the saturation current, and “*a*” is a dimensionless parameter characterizing the properties of metal contacts on highly resistive *h*-BN. Fitting experimental data with Eq. (3) yields a $\mu\tau$ value of $6.4 \times 10^{-5} \text{ cm}^2/\text{V}$. $\mu\tau$ is lower than the typical value of $(1\text{--}2) \times 10^{-4} \text{ cm}^2/\text{V}$ observed in 100 μm thick wafers produced by HVPE.²² We believe that the reduction in $\mu\tau$ in the 1 mm thick wafer is attributed to a degradation in the crystalline quality with wafer thickness. The photocurrent rises rapidly at lower voltages and then starts to saturate at higher voltages, indicating that the charge carrier collection efficiency approaches its maximum limit at higher applied fields. For the 1.3 mm wide detector used here, the results shown in Fig. 3 imply that the applied voltage needs to be above 250 V to ensure an adequate charge collection efficiency.

Based on Eq. (1), $\eta_i = 1 - e^{-d/\lambda}$, the theoretical (or intrinsic) detection efficiency of the 1 mm thick detector for fast neutrons is 1.9% (1.3%) for fast neutrons emitted from the AmBe (Cf-252) source, using $d = 1 \text{ mm}$ and $\lambda = 5.2 \text{ cm}$ (7.6 cm). To experimentally determine the detection efficiency of *h*-BN for fast neutrons, bare Cf-252 and AmBe neutron sources (without an HDPE moderator) were utilized. The inset of Fig. 4 plots the neutron emission spectra of Cf-252 (red curve) and AmBe (blue curve) sources, presenting in the form of the neutron emission rate as a function of neutron energy, E_N . Neutrons emitted from the Cf-252 and AmBe sources have energy ranges of $E_N = 0\text{--}10$ and $E_N = 0\text{--}11 \text{ MeV}$, with average neutron energies of $\langle E_N \rangle = 2.13$ and $\langle E_N \rangle = 4.2 \text{ MeV}$, respectively.

The detector was placed at a distance of 5 cm from the source and operated in such a way as to perform particle counting and pulse height spectrum (PHS) analysis. At a distance of 5 cm from the source, the neutron flux received by the detector can be calculated from $\frac{\text{neutron emission rate (n/s)}}{4\pi R^2}$, where *R* is the distance between the neutron source and the detector. Hence, the AmBe source (with a neutron emission rate of $6.5 \times 10^5 \text{ n/s}$) and Cf-252 source (with a neutron emission rate of $4.7 \times 10^5 \text{ n/s}$) produce, respectively, a neutron flux of 2070 and $1470 \text{ n/s}\cdot\text{cm}^2$ on the detector. Figure 4 plots the PHS of the 1 mm thick *h*-BN detector in response to fast neutrons emitted from Cf-252 (red) and AmBe (blue) sources. For each PHS, detector responses were recorded over four separate 15-min intervals, and the resulting PHS

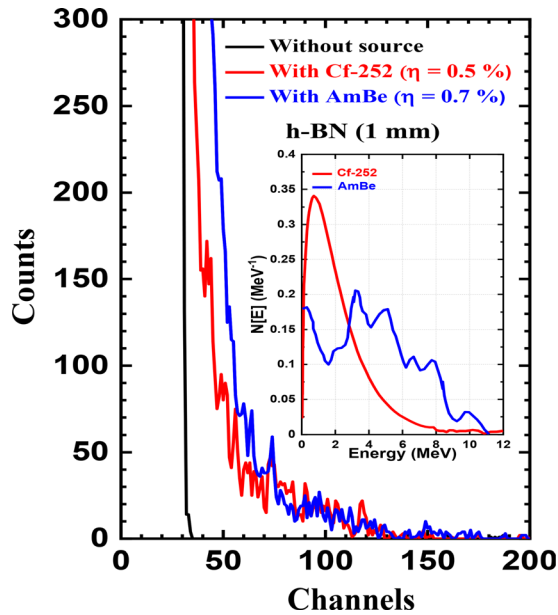


FIG. 4. Pulse height spectra (PHS) measured for a 1 mm thick *h*-BN fast neutron detector in response to fast neutrons emitted from the bare Cf-252 source (red) and AmBe source (blue) at an applied voltage of 450 V. The black spectrum corresponds to the PHS measured at 450 V in the absence of any source (or background counts). The inset plots the neutron emission spectra of Cf-252 (red) and AmBe (blue) neutron sources, indicating that the average energy of neutrons from the AmBe source is higher than that from the Cf-252 source.

shown in Fig. 4 represents the average of these four measurements. The black PHS shown in Fig. 4 represents the background signal, measured in the absence of any neutron source. Over a 15-min measurement time period, the average neutron counts acquired by the *h*-BN detector were 803 neutrons for the AmBe source and 450 neutrons for the Cf-252 source. These data provide overall detection efficiencies of $\eta = \frac{\text{detector's count rate per unit area}}{\text{neutron flux received by the detector}} = \frac{803/(15 \times 60 \times (0.13 \times 0.5))}{2070} = 0.66\%$ for fast neutrons emitted from the AmBe source and $\eta = \frac{450/(15 \times 60 \times (0.13 \times 0.5))}{1470} = 5.2\%$ for fast neutrons emitted from the Cf-252 source, corresponding to a charge collection efficiency of about $\eta_c = 38\%$, where η_c is defined as the ratio of the measured detection efficiency (η) to the intrinsic detection efficiency (η_i) and $\eta_i = 1.9\%$ (1.3%) for fast neutrons emitted from the AmBe (Cf-252) source. It is important to note that the dark currents of the detector and lower-level discrimination (LLD) settings of the electronics were monitored after each PHS measurement and remained stable throughout. This ensures the validity of comparative detection efficiency analysis between AmBe and Cf-252 neutron sources.

Notably, the measured mean free mean path is shorter, and detection efficiency is higher for fast neutrons emitted from the AmBe source than the Cf-252 source. This can be attributed to the fact that these two sources have different neutron emission spectra as shown in the inset of Fig. 4 and the AmBe source has a larger average neutron energy. After elastic scattering, the energy is transferred from fast neutrons to recoil B or N ions, which generate charge carriers. The recoil energy (E_R) can be described as

$$E_R = [4A/(1+A)^2](\cos^2\theta_s)E_N, \quad (4)$$

where A is the atomic number and θ_s is the scattering angle. E_R decreases with A . The total number of electrons (N_e) and holes (N_h) generated from the recoil energies of B and N ions can be expressed as^{28,29}

$$N_e = N_h = E_R/3E_g, \quad (5)$$

where E_g is the energy bandgap of *h*-BN. However, E_R is directly proportional to E_N . As a result, more charge carriers are collected above the LLD, leading to a higher detection efficiency in response to neutrons from the AmBe source compared to the Cf-252 source.

Although the results shown in Fig. 4 represent a significant improvement compared to our previous 90 μm thick *h*-BN fast neutron detectors with a detection efficiency of 0.1% in response to a Cf-252 source, attributing primarily to the increased thickness of the *h*-BN wafers and hence the intrinsic detection efficiency, the charge collection efficiency of these 1 mm thick detectors is significantly lower than a value of about 80% for the 90 μm thick detectors.²⁶ We believe that this is attributed to the degradation of the electronic quality of *h*-BN with increasing layer thickness. To gain insight into the evolution of the electronic quality with wafer thickness, we carried out $\mu\tau$ product measurements as a function of wafer thickness by successively removing *h*-BN materials from top by polishing. As illustrated in Fig. 5(a), with each step of removal of the top *h*-BN layer, the $\mu\tau$ product was monitored. Figure 5(b) plots the measured $\mu\tau$ product vs the sample thickness, which shows a systematic increase in $\mu\tau$ with successive removal of *h*-BN layers from the top surface. We also measured the $\mu\tau$ product of the bottom surface (the surface originally in contact with sapphire prior to lift-off), corresponding to a thickness of $d = 0$. The results shown in Fig. 5 clearly show that the overall electronic properties of *h*-BN declined with increasing *h*-BN thickness.

This observation of material quality deteriorating with increasing *h*-BN layer thickness is in contrast to the case in AlN epilayers, which tend to exhibit a higher crystalline quality with increasing the epilayer thickness. The crystalline quality enhancement with epilayer thickness of AlN was thought to be due to the termination of edge type dislocations by forming loops with similar neighboring dislocations having opposite Burger vector \mathbf{b} as the epilayer thickness increases.³⁰ This suggests that the mechanisms of dislocation formation and structural defects propagation during the growth are different among *h*-BN and AlN, although the two material systems have many similarities in terms of chemical reactions during the growth. In *h*-BN, the stacking sequence has only a minor effect on the total energy of the layer-structured BN crystals.³¹ The inclusion of various polytype domains and structural disorders seems to become more prevalent with increasing the layer thickness during *h*-BN growth. There is a need to further develop an improved understanding of the growth mechanisms of *h*-BN so that high crystalline quality can be retained for *h*-BN quasi-bulk crystals with a thickness exceeding 1 mm. Based on the results of AlN quasi-bulk crystals growth by HVPE,^{32,33} developing high temperature HVPE growth capability is highly desired for further advancing the crystalline quality of *h*-BN quasi-bulk crystals.

In summary, quasi-bulk *h*-BN wafers (1 mm thick) have been produced using HVPE growth method. Detectors fabricated from these wafers demonstrated fast neutron detection efficiencies of 0.7% and 0.5% for AmBe and Cf-252 sources, respectively. Our analysis,

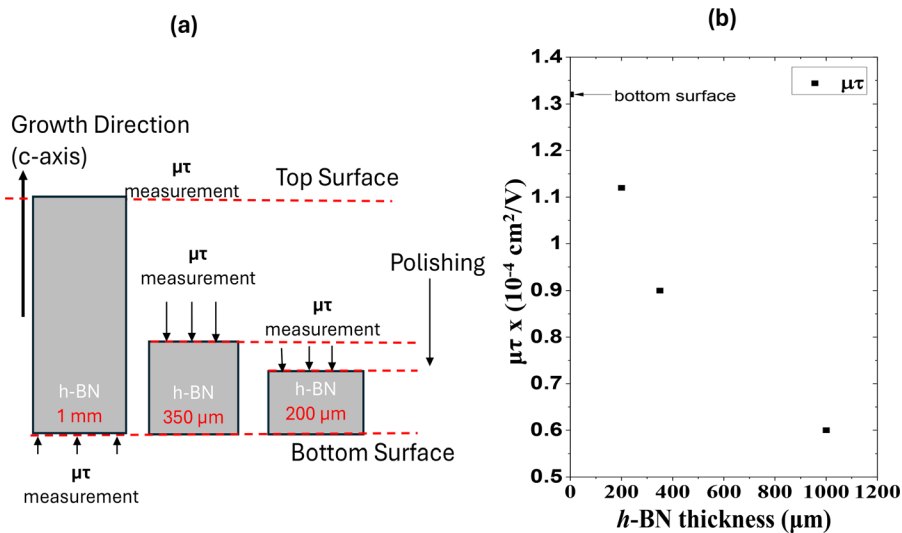


FIG. 5. (a) Schematic diagram of removing *h*-BN material from the top surface by polishing. (b) $\mu\tau$ product vs the remaining *h*-BN thickness.

involving layer-by-layer polishing, showed that charge collection efficiency is affected by a decline in the carrier mobility-lifetime ($\mu\tau$) product as the material thickness increases. We attribute this decline in $\mu\tau$ to an increase in structural disorders that accumulate during thicker layer growth. Therefore, enhancing the $\mu\tau$ product in thick *h*-BN by minimizing these structural defects is the critical next step. While further optimization is needed, this study provides a crucial foundation for developing direct conversion neutron detection technologies, which have a significant potential impact across diverse fields like nuclear safety and monitoring, security, energy exploration, medical applications (imaging/therapy), and basic materials science research.

The information, data, or work presented herein was funded in part by the Advanced Research Projects Agency-Energy (ARPA-E), U.S. Department of Energy, under Award No. DE-AR0001552 monitored by Dr. Olga Spahn and Dr. Eric Carlson. The views and opinions of authors expressed herein do not necessarily state or reflect those of the United States Government or any agency thereof. Jiang and Lin are grateful to the AT&T Foundation for the support of Ed Whitacre and Linda Whitacre endowed chairs.

AUTHOR DECLARATIONS

Conflict of Interest

The authors have no conflicts to disclose.

Author Contributions

G. Somasundaram: Data curation (equal); Formal analysis (equal); Methodology (equal); Software (equal); Validation (equal); Visualization (equal); Writing – original draft (equal). **N. K. Hossain:** Data curation (equal); Formal analysis (equal); Investigation (equal); Methodology (equal); Software (equal); Validation (equal); Visualization (equal). **Z. Alemoush:** Data curation (equal); Formal analysis (equal); Investigation (equal); Methodology (equal); Software (equal); Validation (equal); Visualization (equal). **A. Tingsuwatit:** Data curation (equal); Formal analysis (equal); Investigation (equal); Methodology (equal); Software (equal); Validation (equal);

Visualization (equal). **J. Li:** Data curation (equal); Formal analysis (equal); Investigation (equal); Methodology (equal); Project administration (equal); Resources (equal); Software (equal); Supervision (equal); Validation (equal); Visualization (equal). **J. Y. Lin:** Conceptualization (equal); Formal analysis (equal); Funding acquisition (equal); Investigation (equal); Methodology (equal); Project administration (equal); Resources (equal); Supervision (equal); Validation (equal); Visualization (equal); Writing – review & editing (equal). **H. X. Jiang:** Conceptualization (equal); Formal analysis (equal); Funding acquisition (equal); Investigation (equal); Methodology (equal); Project administration (equal); Resources (equal); Supervision (equal); Validation (equal); Visualization (equal); Writing – original draft (equal); Writing – review & editing (equal).

DATA AVAILABILITY

The data that support the findings of this study are available within the article.

REFERENCES

- A. K. Geim and I. V. Grigorieva, “Van der Waals heterostructures,” *Nature* **499**, 419 (2013).
- R. Bourrellier, S. Meuret, A. Tararan, O. Stephan, M. Kociak, L. H. G. Tizei, and A. Zobelli, “Bright UV single photon emission at point defects in *h*-BN,” *Nano Lett.* **16**, 4317 (2016).
- T. Sugino, K. Tanioka, S. Kawasaki, and J. Shirafuji, “Characterization and field emission of sulfur-doped boron nitride synthesized by plasma-assisted chemical vapor deposition,” *Jpn. J. Appl. Phys., Part 2* **36**, L463 (1997).
- K. Watanabe, T. Taniguchi, and H. Kanda, “Direct-bandgap properties and evidence for ultraviolet lasing of hexagonal boron nitride single crystal,” *Nat. Mater.* **3**, 404 (2004).
- B. Arnaud, S. Lebègue, P. Rabiller, and M. Alouani, “Huge excitonic effects in layered hexagonal boron nitride,” *Phys. Rev. Lett.* **96**, 026402 (2006).
- Y. Kubota, K. Watanabe, O. Tsuda, and T. Taniguchi, “Deep ultraviolet light-emitting hexagonal boron nitride synthesized at atmospheric pressure,” *Science* **317**, 932 (2007).
- G. Cassabois, P. Valvin, and B. Gil, “Hexagonal boron nitride is an indirect bandgap semiconductor,” *Nat. Photonics* **10**, 262 (2016).
- Y. Hattori, T. Taniguchi, K. Watanabe, and K. Nagashio, “Anisotropic dielectric breakdown strength of single crystal hexagonal boron nitride,” *ACS Appl. Mater. Interfaces* **8**, 27877 (2016).

- ⁹Y. Hattori, T. Taniguchi, K. Watanabe, and K. Nagashio, "Comparison of device structures for the dielectric breakdown measurement of hexagonal boron nitride," *Appl. Phys. Lett.* **109**, 253111 (2016).
- ¹⁰C. Yuan, J. Li, L. Lindsay, D. Cherns, J. W. Pomeroy, S. Liu, J. H. Edgar, and M. Kuball, "Modulating the thermal conductivity in hexagonal boron nitride via controlled boron isotope concentration," *Commun. Phys.* **2**, 43 (2019).
- ¹¹A. Maity, S. J. Grenadier, J. Li, J. Y. Lin, and H. X. Jiang, "Hexagonal boron nitride: Epitaxial growth and device applications," *Prog. Quantum Electron.* **76**, 100302 (2021).
- ¹²P. Vuong, T. Moudakir, R. Gujrati, A. Srivastava, V. Ottapilakkal, S. Gautier, P. L. Voss, S. Sundaram, J. P. Salvestrini, and A. Ougazzaden, "Scaling up of growth, fabrication, and device transfer process for GaN-based LEDs on h-BN templates to 6-inch sapphire substrates," *Adv. Mater. Technol.* **8**, 2300600 (2023).
- ¹³T. S. Cheng, A. Summerfield, C. J. Mellor, A. Davies, A. N. Khlobystov, L. Eaves, C. T. Foxon, P. H. Beton, and S. V. Novikov, "High-temperature molecular beam epitaxy of hexagonal boron nitride layers," *J. Vac. Sci. Technol. B* **36**, 02D103 (2018).
- ¹⁴D. A. Laleyan, K. Mengle, S. Zhao, Y. Wang, E. Kioupakis, and Z. Mi, "Effect of growth temperature on the structural and optical properties of few-layer hexagonal boron nitride by molecular beam epitaxy," *Opt. Express* **26**, 23031 (2018).
- ¹⁵Z. Xu, H. Tian, A. Khanaki, R. Zheng, M. Suja, and J. Liu, "Large-area growth of multi-layer hexagonal boron nitride on polished cobalt foils by plasma-assisted molecular beam epitaxy," *Sci. Rep.* **7**, 43100 (2017).
- ¹⁶S. F. Chichibu, K. Shima, K. Kikuchi, N. Umehara, K. Takiguchi, Y. Ishitani, and K. Hara, "Recombination dynamics of indirect excitons in hexagonal BN epilayers containing polytypic segments grown by chemical vapor deposition using carbon-free precursors," *Appl. Phys. Lett.* **120**, 231904 (2022).
- ¹⁷O. Osberghaus, "Die Isotopenhäufigkeit des Bors. Massenspektrometrische untersuchung der elektronenstoßprodukte von BF_3 und BCl_3 ," *Z. Phys.* **128**, 366 (1950).
- ¹⁸G. F. Knoll, *Radiation Detection and Measurement*, 4th ed. (John Wiley & Sons, 2010).
- ¹⁹A. Maity, S. J. Grenadier, J. Li, J. Y. Lin, and H. X. Jiang, "Toward achieving flexible and high sensitivity hexagonal boron nitride neutron detectors," *Appl. Phys. Lett.* **111**, 033507 (2017).
- ²⁰A. Maity, S. J. Grenadier, J. Li, J. Y. Lin, and H. X. Jiang, "High sensitivity hexagonal boron nitride lateral neutron detectors," *Appl. Phys. Lett.* **114**, 222102 (2019).
- ²¹A. Maity, S. J. Grenadier, J. Li, J. Y. Lin, and H. X. Jiang, "High efficiency hexagonal boron nitride neutron detectors with 1 cm^2 detection areas," *Appl. Phys. Lett.* **116**, 142102 (2020).
- ²²Z. Alemoush, A. Tingsuwatit, A. Maity, J. Li, J. Y. Lin, and H. X. Jiang, "Status of h-BN quasi-bulk crystals and high efficiency neutron detectors," *J. Appl. Phys.* **135**, 175704 (2024).
- ²³See <https://www.nrc.gov/docs/ML1122/ML11229A705.pdf> for "Interactions of Neutrons with Matter."
- ²⁴See <https://www.osti.gov/servlets/purl/7329788> for "Light Element Standard Cross Sections for ENDF/B."
- ²⁵J. Li, A. Tingsuwatit, Z. Alemoush, J. Y. Lin, and H. X. Jiang, "Ultrawide bandgap semiconductor h-BN for direct detection of fast neutrons," *APL Mater.* **13**, 011101 (2025).
- ²⁶A. Tingsuwatit, A. Maity, S. J. Grenadier, J. Li, J. Y. Lin, and H. X. Jiang, "Boron nitride neutron detector with the ability for detecting both thermal and fast neutron," *Appl. Phys. Lett.* **120**, 232103 (2022).
- ²⁷A. Tingsuwatit, N. K. Hossain, Z. Alemoush, M. Almohammad, J. Li, J. Y. Lin, and H. X. Jiang, "Properties of photocurrent and metal contacts of highly resistive ultrawide bandgap semiconductors," *Appl. Phys. Lett.* **124**, 162105 (2024).
- ²⁸C. A. Klein, "Bandgap dependence and related features of radiation ionization energies in semiconductors," *J. Appl. Phys.* **39**, 2029 (1968).
- ²⁹S. T. Pantelides, D. G. Walker, R. Mahmud, M. V. Fischetti, and R. D. Schrimpf, "The foundations of Shockley's equation for the average electron-hole-pair creation energy in semiconductors," *Appl. Phys. Lett.* **121**, 042104 (2022).
- ³⁰B. N. Pantha, R. Dahal, M. L. Nakarmi, N. Nepal, J. Li, J. Y. Lin, H. X. Jiang, Q. S. Paduano, and D. Weyburne, "Correlation between optoelectronic and structural properties and epilayer thickness of AlN," *Appl. Phys. Lett.* **90**, 241101 (2007).
- ³¹K. A. Mengle and E. Kioupakis, "Impact of the stacking sequence on the bandgap and luminescence properties of bulk, bilayer, and monolayer hexagonal boron nitride," *APL Mater.* **7**, 021106 (2019).
- ³²Y. Kumagai, T. Yamane, and A. Koukitu, "Growth of thick AlN layers by hydride vapor-phase epitaxy," *J. Cryst. Growth* **281**, 62 (2005).
- ³⁵Y. Kumagai, K. Goto, T. Nagashima, R. Yamamoto, M. Bockowski, and J. Kotani, "Influence of growth rate on homoepitaxial growth of AlN at 1450°C by hydride vapor phase epitaxy," *Appl. Phys. Express* **15**, 115501 (2022).